25 April 1980, Volume 208, Number 4442 SCIENCE

Computer Models of Crystal Growth

G. H. Gilmer

Summary. Dynamic models of crystal surfaces have provided new insights into the crystal growth process. The effects of surface roughening, dislocations, and impurities have been assessed. Certain impurities have been found to cause a larger increase in the growth rate than screw dislocations.

This article is concerned with the structure and motion of the interface between a crystal and the surrounding fluid. The growth rate of a crystal is determined by the net deposition rate, the rate at which atoms from the fluid condense at the interface and assume the ordered structure of the crystal. Becker and Döring (*1*) calculated the deposition rate by assuming that new layers of atoms are initiated by a nucleation process. In most cases, however, they predicted infinitesimal deposition rates, many orders of magnitude smaller than those observed in the laboratory. This huge discrepancy between theory and experiment was apparently resolved in 1949, when Frank (*2*) pointed out that screw dislocation lattice defects provide sites on the surface where rapid growth can occur. Since that time, the spiral growth mechanism has been confirmed in a number of instances (*3*). But recent experience with dislocation-free crystals shows that spiral growth is not the only mechanism that leads to fast rates (*4*). Other factors such as the interface temperature and the impurity content of the fluid also can have decisive effects. In this article I describe a simple model of the growing crystal. Simulations of this model provide a definitive test of the early theories and also yield data for more complicated situations such as those characterized by high surface temperatures and impurities.

Computer simulation models have some distinct advantages over the traditional methods for studying crystal growth. During the simulation it is possible to observe and measure the motion of individual atoms and clusters and to measure the average rates of deposition. Computer-generated color movies provide the most dramatic method of observation; the atomic configurations generated during the simulations are represented by computer graphics on a color television monitor and are filmed with a computer-controlled camera (*5*). I illustrate here some typical configurations with microfilm drawings. The dynamic properties are indicated by measurements of the average rates of deposition. A disadvantage of the simulation models is the large amount of computation required to explore their properties for a variety of conditions, but the importance of this factor is diminishing as new and more powerful computers are developed.

The kinetic Ising model (*6*) is used in all the simulations described here. It exhibits many of the phenomena observed in the laboratory. First, I consider the reasons behind the distinctive shapes of crystals grown at various temperatures. This topic is related to the surface roughening transition, and I consider the effect of this transition on the growth rate. Then the spiral growth mechanism is assessed, and spiral kinetics are compared with those on a perfect crystal face. Finally, the influence of various impurities is considered. An important new growth mechanism is observed when the impurity segregates at the crystal surface. The capture of impurity in the growing crystal is discussed, together with the growth of metastable alloys.

Kinetic Ising Model

For convenience, I use the terminology of vapor deposition, although most of the results can be applied to the growth of crystals from solution and even to the solidification of a melt. The arrangements of atoms at different surfaces of a simple crystal are depicted in Fig. 1a. Three surface orientations with close-packed layers of atoms on the face-centered-cubic (fcc) lattice are shown. The Ising model of such an interface results from the following assumptions: (i) Atoms are permitted only at fcc lattice sites. (ii) Only one atom is allowed to occupy a site. (iii) Attractive interactions extend only to nearest-neighbor atoms, and the total potential energy is the sum of all such pair interaction energies. A particular configuration can be represented in the computer simply as a list of all occupied sites, and various quantities such as the potential energy can be calculated directly from this list. Further restrictions are usually imposed, such as a requirement that each atom be connected to the crystal by at least one nearest-neighbor interaction or "bond." But under normal crystal growth conditions these restrictions have little effect on the properties of the model. Sections of the crystal somewhat larger than those shown in Fig. 1 are simulated in the computer; typically these sections include a square area with 60 atoms on an edge. Edge effects are eliminated by the use of periodic boundary conditions; that is, atoms at an edge interact with atoms in a replica of the section translated to a position adjacent to the edge.

The dynamics of crystal growth are simulated by two basic events, impingement and evaporation. One chooses an

---

The author is a member of the technical staff at Bell Laboratories, Murray Hill, New Jersey 07974.

0036-8075/80/0425-0355$02.00/0

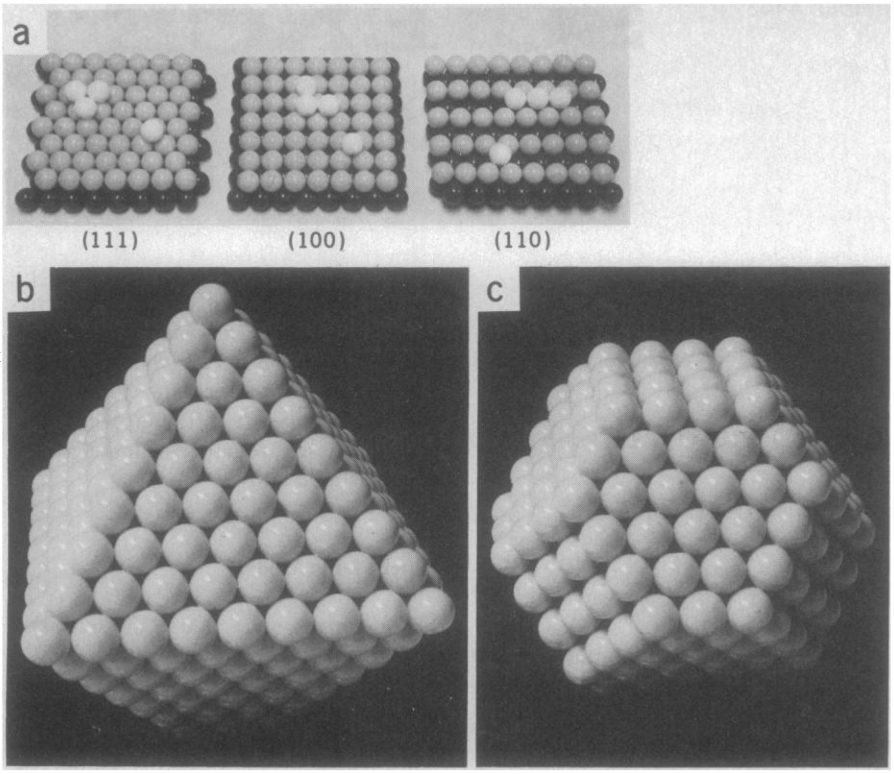

Fig. 1. Ball models for fcc crystals. (a) The models are terminated along the three different low-index orientations with Miller indices as indicated. The darker shades correspond to atoms belonging to layers that are farther removed from the surface, and individual atoms and those belonging to small clusters on the surface are white. (b) Octahedron that results when the crystal is bounded by the eight (111) and equivalent faces. (c) Truncated octahedron with (111) and (100) faces.

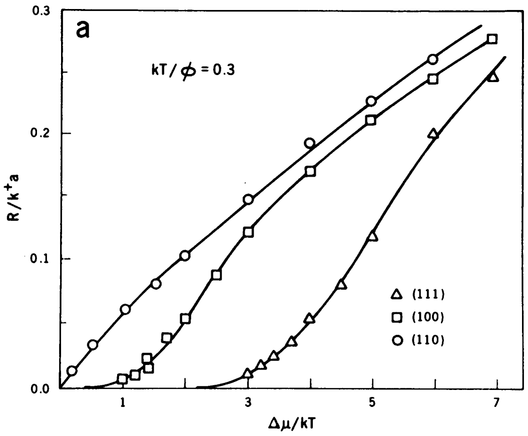

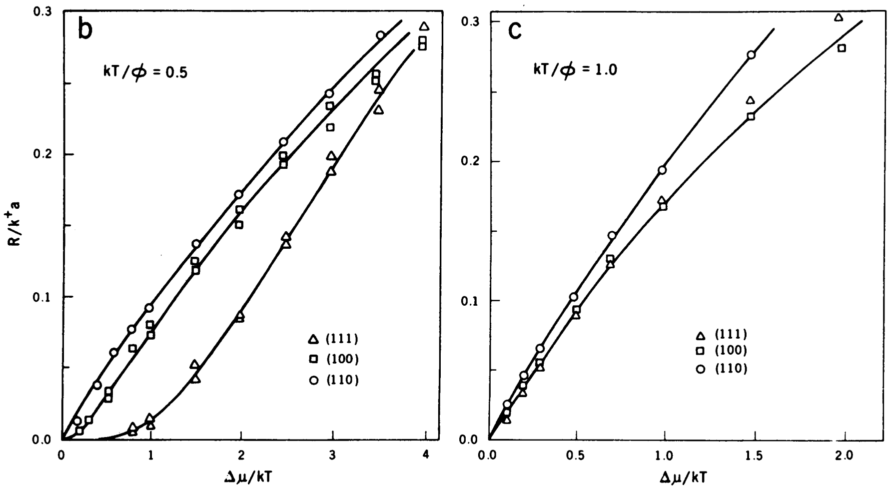

Fig. 2. The simulated growth rates (R) of the three faces shown in Fig. 1 are plotted versus the chemical potential driving force ($\Delta\mu$) at three temperatures: (a) $kT/\phi = 0.3$; (b) $kT/\phi = 0.5$; and (c) $kT/\phi = 1.0$. The calculated speed of the interface is normalized by the factor k^+a, where a is the fcc unit cell length.

event and the site where it is to occur by using a computer-generated random number, in accordance with standard Monte Carlo procedure (*7*). Impingement is the addition of an atom at a site on the surface, and its probability is assumed to be proportional to the supersaturation in the vapor. In terms of the chemical potential, μ, the deposition rate is

$$k^+ = \nu \exp(\mu/kT) \qquad (1)$$

where ν is a frequency factor, T is the absolute temperature, and k is Boltzmann's constant. Here I have used the dilute-solution approximation relating the chemical potential and the concentration C in the vapor, $\mu - \mu^{(e)} = kT \ln C/C^{(e)}$, where the superscript denotes an equilibrium quantity (*8*). The impingement rate is independent of the local surface structure, as expected for a crystal surface in contact with a vapor.

Evaporation is the removal of an atom from the surface region, and it proceeds with a frequency k_n^- that is highly sensitive to the structure:

$$k_n^- = \nu \exp(-n\phi/kT) \qquad (2)$$

where n is the number of bonds to other atoms of the crystal, and ϕ is the energy required to break one bond. In effect, I assume that evaporation is a simple activated process. Equilibrium prevails when the average rate of impingement is balanced by evaporation, so that the number of atoms in the crystal remains essentially constant over long periods of time. The chemical potential required for equilibrium is $\mu^{(e)} = -Z\phi/2$, where Z is the number of nearest neighbors of an atom in the bulk (*9*) ($Z = 12$ for the fcc lattice). The corresponding impingement rate is equal to the rate of evaporation from a surface site with exactly half of the neighbors present, the "kink site" of early theories of crystal growth (*10, 11*). This site is unique because an entire layer of atoms can, in principle, be deposited by sequential deposition only on kink sites. Most crystals grow under conditions where the impingement and evaporation fluxes are nearly equal, and the net rate of accumulation of atoms in the crystal is relatively small.

Habit

The symmetry of a crystal lattice is often reflected in the external shape, or habit, of the crystal. In general, the deposition rates on different segments of the crystal surface may depend on the orientation of the segments relative to the crystal lattice. The characteristic shapes of crystals found in nature are primarily a result of this anisotropy of the deposition rate. Suppose, for example, that a small fcc crystal in the shape of a sphere is placed in an environment that is uniformly supersaturated. All possible orientations are represented on its surface, including those shown in Fig. 1a. If the growth rate were isotropic, the crystal would remain perfectly spherical during growth. Anisotropic growth will cause distortions of this shape, and, if the anisotropy is appreciable, the rapid accumulation of material on the fast growth directions will leave extended flat sections (facets) parallel to the slow growth orientations. The initial shape of the crystal will have little effect on the ultimate product, provided that the initial crystal is relatively small. Very slow growth on the (111) face and equivalent orientations produces an octahedron (Fig. 1b), and a truncated octahedron occurs when the growth rate on the (100) face is nearly equal to that on the (111) face (Fig. 1c).

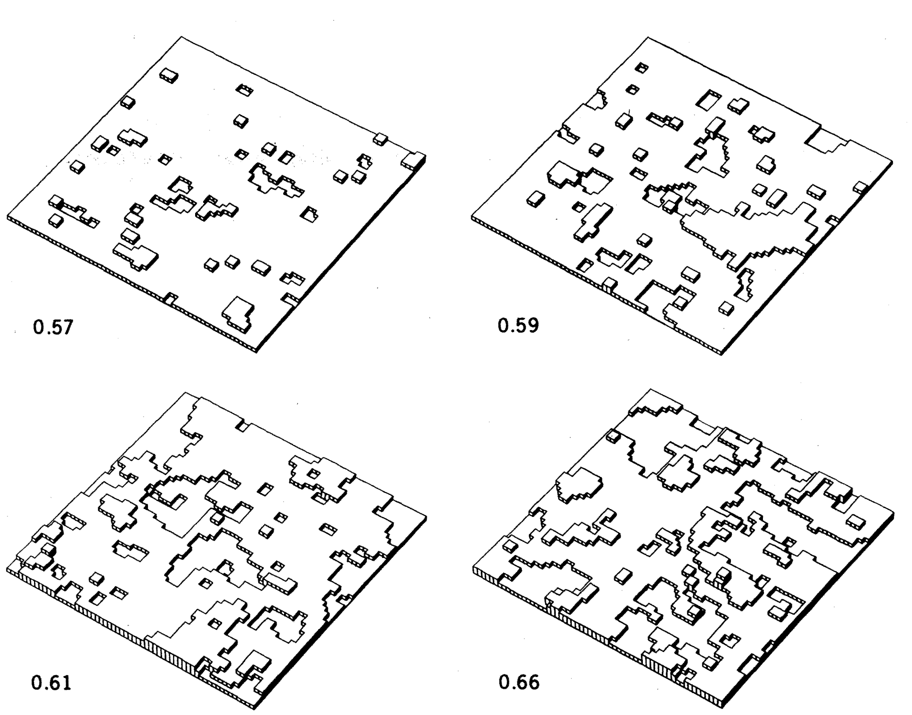

Fig. 3. Typical configurations of the sc (100) face generated by the Monte Carlo simulations in the case of a crystal in equilibrium with its vapor. Atoms are drawn as cubes. Small clusters and atoms with fewer than three bonds and the equivalent vacancy configurations are not represented. The numbers adjacent to the figures indicate the value of kT/ϕ used in the simulations.

Gilmer and Jackson simulated deposition on the three orientations illustrated in Fig. 1a, using the model described above (*12*). We calculated the average growth rates from the net change in the number of particles after the simulation of millions of condensation and evaporation events. These rates are plotted in Fig. 2 as a function of the chemical potential driving force, $\Delta\mu = \mu - \mu^{(e)}$, and at three different temperatures. Two distinct types of kinetics are apparent from the data: (i) Continuous growth usually occurs at high temperatures (Fig. 2c) and is characterized by a linear dependence of the growth rate on $\Delta\mu$. In this case even the close-packed (111) plane offers little impediment to the condensation of atoms. (ii) Nucleation kinetics occur at low temperatures on the (111) and (100) faces (Fig. 2a); in this case the growth rate remains essentially zero for small positive values of $\Delta\mu$. (We have included a large range of $\Delta\mu$ values in Fig. 2, but most crystals are actually grown at values less than $0.5\,kT$ and values of $0.01\,kT$ are common during growth from solution. Very large values may exist in molecular beam systems, however.) Large kinetic anisotropy occurs at the lower temperatures where some facets exhibit nucleation kinetics, but growth is nearly isotropic at $kT/\phi = 1.0$, where the continuous mechanism is operative on all three faces.

When $\Delta\mu$ is smaller than $2\,kT$, the (111) face is essentially immobile at the lowest temperature (Fig. 2a). Since the other orientations have appreciable growth rates at values of $\Delta\mu > kT$, a perfect single crystal growing in the range $kT < \Delta\mu < 2\,kT$ would expand quickly until it assumed an octahedral shape. At this point, all measurable growth would cease. Indeed, octahedral crystals are observed in supersaturated vapors of certain fcc metals (*13*). When $\Delta\mu > 5\,kT$, other planes have growth rates within about a factor of 2 of that of the (111) face, and the habit of the crystal may also include facets corresponding to these directions.

The variations in growth rates are related to the different atomic configurations shown in Fig. 1a. Atoms on the (111) face have fewer nearest-neighbor bonds than atoms on the (100) or (110) faces. A single atom, or adatom, on a perfect (111) face has three bonds, on the (100) face it has four, and on the (110) face it has five (see Fig. 1a). Thus, although each face experiences the same incident flux, the atoms that attach to the (110) face, for example, do not evaporate as readily as those on the (100) and (111) faces (see Eq. 2). The relative ability to retain impinging atoms accounts qualitatively for the simulation results; it correctly predicts which faces have the fastest and slowest growth rates.

The (111) and (100) faces can exist in a state of metastable equilibrium with a slightly supersaturated vapor for long periods of time. The density of adatoms remains low on these faces because of their relatively fast evaporation rate. Most atoms impinging at low temperatures produce adatoms, and hence an approximate expression for the adatom density is obtained by equating the impingement rate k^+ and the adatom evaporation rate,

$$\rho_m = k^+/k_m^- \qquad (3)$$

where ρ_m is the probability of finding an adatom on one of the sites and m is 3 or 4 for the (111) and (100) faces, respectively. From Eqs. 1, 2, and 3 we find that $\rho_3 = 4.54 \times 10^{-5}$ and $\rho_4 = 1.27 \times 10^{-3}$ at $kT/\phi = 0.3$ and with $\Delta\mu = 0$. These faces remain very smooth and flat in equilibrium, and even a small supersaturation does not change their structure appreciably.

However, a few clusters are generated on these faces by a fortuitous series of impingement events on neighboring sites. A very small cluster is more likely to disintegrate than to expand, since atoms at its periphery are only weakly bonded to the crystal. But occasionally a cluster may appear that is larger than the critical size for nucleation; this cluster is more likely to continue growing because of the stabilizing influence of the bonds within the cluster itself. Although the formation of a critical cluster may be rare, once such a cluster is formed it can grow until it covers the entire face of the crystal.

The size of the critical cluster depends on the binding energy of atoms on the crystal face, and on $\Delta\mu$. A large binding energy slows evaporation and favors small critical clusters, hence the (100) kinetics are faster than (111). Likewise, a large value of $\Delta\mu$ increases k^+, and the diameter of the critical cluster is found to be inversely proportional to $\Delta\mu$ (*1*). Simulation data on cluster nucleation are in accord with a modified form of the early nucleation theory (*14, 15*). When $\Delta\mu$ is very small, the critical cluster size is large and the probability of generating such a cluster is minute.

The (110) face has quite different kinetic properties. Consider a cluster of two atoms on neighboring sites (in the same row of Fig. 1). Each atom in the cluster has six bonds, five to atoms in the layers below and one to the other atom in the cluster, and therefore each has the kink site evaporation rate. But the impingement rate on the two sites at the ends of the pair is larger by a factor of exp $(\Delta\mu/kT)$ according to Eq. 1, and hence a pair of adatoms is stable at any positive value of $\Delta\mu$. Thus large clusters are not necessary, and the probability of generating a critical nucleus is significant at all values of $\Delta\mu$. For this reason measurable growth rates are observed for any $\Delta\mu > 0$. This property in general applies to all surfaces except the close-packed orientations, where the atoms are connected by a two-dimensional network of bonds.

The simulation results for the (111) and (100) faces seem to imply that these faces grow by a nucleation mechanism at low temperatures, and that there is a transition to continuous growth at high temperatures. Nucleation is apparently not necessary above a critical temperature that depends on the crystal face. The possibility of such a surface phase transition at a specific temperature has been debated for a number of years. Burton and Cabrera (*16*) and Jackson (*17*) approached this question by investigating models for the structure of the interface under equilibrium conditions. In both cases, an Ising model was used to represent only one layer of sites on the surface of a perfect crystal. These investigators showed that this layer is exactly equivalent to a two-dimensional (2d) model. They concluded from the known properties of this latter system that a definite surface roughening temperature should exist, corresponding to the phase transition that occurs at the critical temperature, $T_c^{(2d)}$. Far below this temperature, the surface layer contains only a small number of adatoms and a few clusters, and Eq. 3 is accurate. But as $T \rightarrow T_c^{(2d)}$, the occupancy of the surface layer approaches 50 percent. These researchers assumed that nucleation kinetics would exist only below $T_c^{(2d)}$, since above this point large clusters are always present as a basic part of the interface structure.

Although the 2d Ising model of the interface provides suggestive evidence for a roughening transition, the restriction to a single layer places a severe constraint on the system. This restriction was removed in the diffuse interface theory of Cahn and Hilliard (*18*), where the density of the interfacial region was represented by a continuous function of the vertical coordinate. Surprisingly, this theory predicted that a region of metastable equilibrium persists at all temperatures, although it is confined to very small values of $\Delta\mu$ at high temperatures. A roughening transition is not present, and highly anisotropic growth is always possible if the driving force is sufficiently small. Temkin (*19*) extended Jackson's model to a multilevel interface and also found that the roughening transition was suppressed. However, in both of these models the mean field (Bragg-Williams) approximation was used, and this method assumes a random distribution of atoms in each layer (*8*). The preferential clustering of atoms as a result of the interaction between neighbors is not correctly treated. For this reason, mean field methods give unphysical results in situations where the particles tend to form compact clusters; for example, zero growth rates are calculated for the interface models over an appreciable range of driving force (*19*). Thus, these theories cannot be trusted.

Later, multilevel models of the interface were examined by means of the Monte Carlo method (*20*). A transition from nucleation to continuous growth was suggested by a calculation of deposition rates on the simple cubic (sc) (100) face (*21*); these results are similar to the more recent data presented above for the fcc (100) face. Furthermore, it was found that the equilibrium interface was delocalized at high temperatures (*9*). At

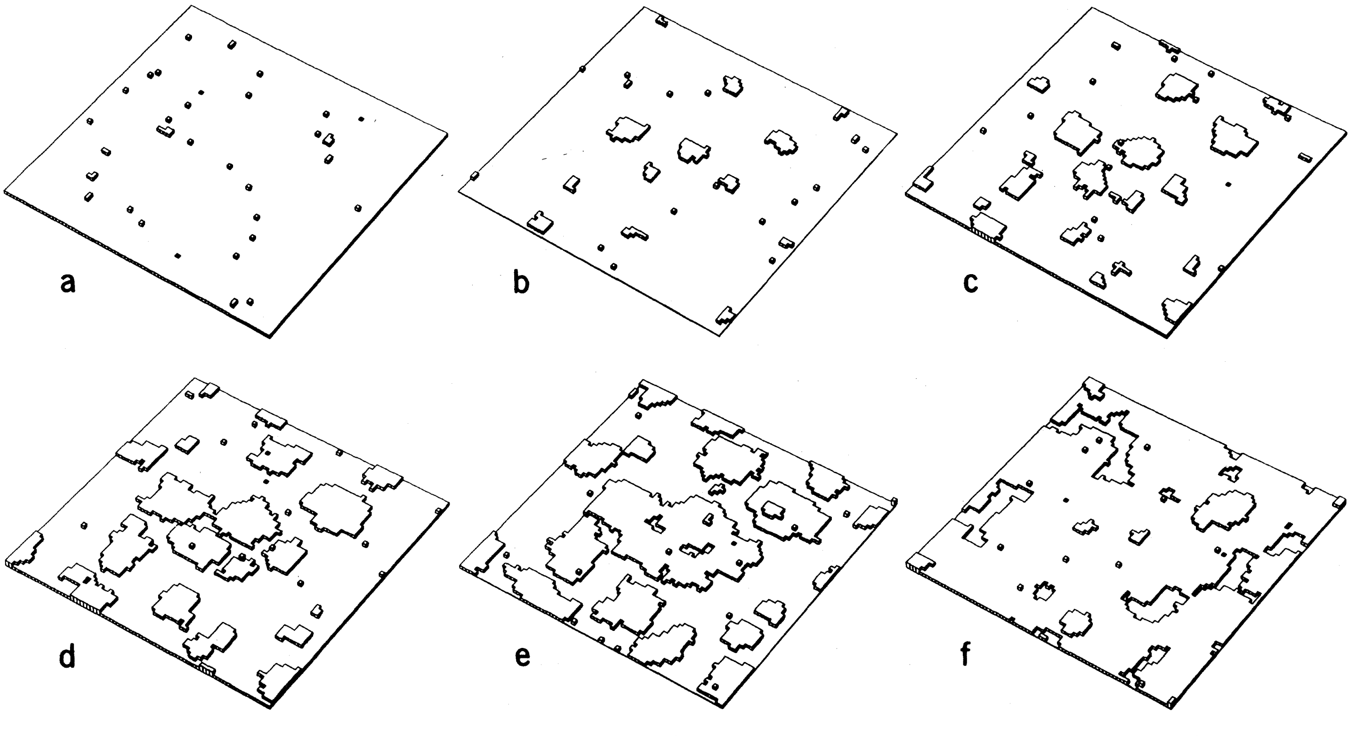

Fig. 4. Configurations of an sc (100) face during an initial transient period of growth (see text). Here $kT/\phi = 0.25$ and $\Delta\mu/kT = 2$.

low temperatures, where nucleation kinetics were observed, the equilibrium interface appeared to be pinned at one lattice plane and the average height of the surface never changed by more than a small fraction of the distance between close-packed layers. At the higher temperatures, however, the interface was no longer stationary and the average height was observed to fluctuate through large distances. Some of the configurations generated by the Monte Carlo method are shown in Fig. 3, where the (100) face of an sc lattice is in equilibrium with the vapor. [Because of the square arrangement of atoms in the surface layer, the kinetics and equilibrium properties of this face are nearly identical to those of the fcc (100) face discussed above.] Below the roughening temperature, T_R, clusters of adatoms and vacancies are of limited size, whereas above T_R clusters that extend across most of the simulated region are present. The random growth and decay of these clusters permit the interface to move in the vertical direction. Moreover, these clusters provide stable nuclei when exposed to a supersaturated vapor, and for this reason the crystal can grow continuously without the need for nucleation.

The first theoretical approach in agreement with this picture was given by Weeks *et al.* (*22*). They pointed out that the interface density profile must vanish when the interface becomes delocalized. A low-temperature series for the profile width was calculated, and series extrapolations indicated that the width diverges at a temperature slightly above $T_c^{(2d)}$. This result and the Monte Carlo data provided rather convincing evidence that the multilevel interface does exhibit a roughening transition.

The most definitive theoretical evidence is now provided by work relating the multilevel interface model to other systems with confirmed phase transitions. Chui and Weeks (*23*) obtained a direct relation to the metal-insulator transition in a two-dimensional Coulomb gas, and van Beijeren (*24*) derived a relation to the phase transition in the six-vertex or F model. These results confirm the predicted divergence of the interface profile width and show that thermodynamic quantities such as the specific heat do not exhibit anomalous behavior near T_R.

Recent experiments have clearly shown the practical consequences of the roughening transition. A complete disappearance of facets on vapor-grown crystals has been observed at temperatures well below the melting point. Jackson and Miller (*25*) observed a drastic change in the morphology of hexachloroethane crystals above 100°C and also in ammonium chloride above 160°C. Similar results were found recently by Pavlovska for adamantane crystals (*26*).

Transients

More information about the interface kinetics can be derived from the transient response of an interface to the sudden application of a driving force. For this study, a crystal initially in equilibrium with its vapor is suddenly placed in a supersaturated region and the subsequent deposition rate is monitored. Such experiments were first performed with electrocrystallization systems, where the driving force can be applied by means of an external potential on the electrodes and the current is proportional to the rate of crystallization (*27*). Some of the configurations that occur during a Monte Carlo simulation of this process are illustrated in Fig. 4. The corresponding equilibrium surface is quite smooth, with only a few adatoms and vacancies. In the presence of the driving force, clusters are generated at various places on the crystal surface. This series of pictures indicates that a number of stable clusters are nucleated in each layer. (In this case the critical cluster contains about five atoms.) The layer is completed when the clusters merge with one another and fill up all the remaining holes.

The average rates of deposition during the transient period are shown in Fig. 5, where $t = 0$ is the time at which the driving force was applied (*28*). The curve with the lowest indicated temperature ($kT = 0.25\phi$) corresponds to the conditions of Fig. 4. The initial rates are small in this case, before many stable clusters have been deposited. At that time, most of the atoms impinging on the surface produce adatoms that quickly evaporate. As stable clusters nucleate and spread, the growth rates increase and reach a maximum when about two-thirds of a monolayer is deposited. The subsequent minimum occurs shortly after a monolayer of material has been added. At this point many of the clusters in the first layer have merged, and nucleation at the second level has not progressed very far (see Fig. 4f). Later, after clusters in the second layer have expanded, a second maximum occurs, and the damped oscillations indicate the deposition of successive layers.

The random nature of the impingement and nucleation processes causes local regions of the crystal surface to experience different rates of deposition. As a result, the surface becomes distributed over many levels and the local regions reach their maximum growth rates at different times. This leads to a time-independent asymptotic rate. The amplitude of the growth rate oscillations is a measure of the extent to which the interface is localized.

The roughening transition is reflected

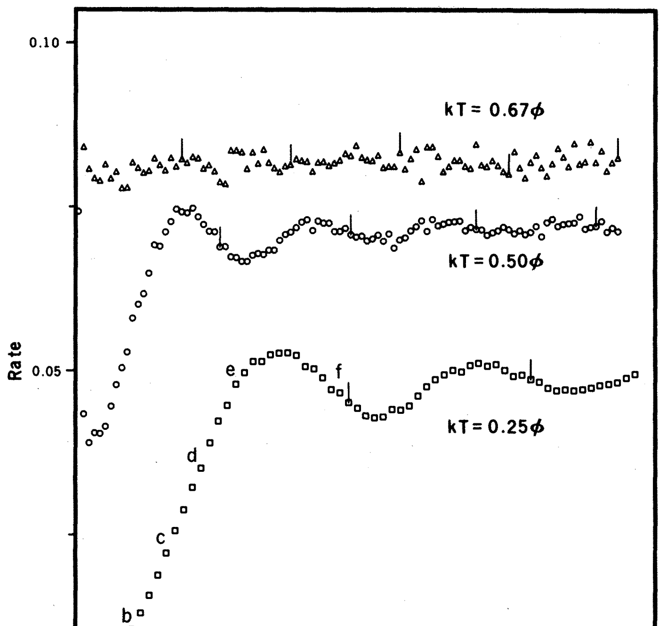

Fig. 5. Transient growth rates of the sc (100) face. The data points plotted are the average desposition rates during the time intervals after the driving force is applied. Each data point represents an average of 50 to 100 simulations on 60 by 60 segments. Vertical lines on the data points indicate the completion of a new layer. The letters next to the data for $kT/\phi = 0.25$ indicate the approximate times at which the corresponding pictures in Fig. 4 were taken. The driving force was chosen in each case to give approximately equal asymptotic growth rates; $\Delta\mu/kT = 2$ when $kT/\phi = 0.25$; $\Delta\nu/kT = 0.6$ when $kT/\phi = 0.50$; and $\Delta\mu/kT = 0.5$ when $kT/\phi = 0.67$.

in the transients at high temperature that are shown in Fig. 5. At $kT/\phi = 0.50$, the transient is qualitatively similar to that at the lower temperature, although the amplitude of the oscillations is smaller and the first minimum is considerably larger. The equilibrium surface at this temperature has many small clusters of adatoms and vacancies, and the edges of these clusters afford sites where the impinging atoms can attach securely to the crystal. The transient at $kT/\phi = 0.67$ exhibits only a short initial decrease to a constant, steady-state growth rate. There is no evidence of nucleation, and again these results imply a transition from nucleation to continuous growth. The transition occurs between $kT = 0.50\phi$ and $kT = 0.67\phi$, precisely the region where the change in the equilibrium structure was observed (Fig. 3). Transients similar to the low-temperature case have been measured in electrodeposition experiments (*27*), but the gradual diminishing of the oscillations with increasing temperature has not yet been observed.

Spiral Growth

My discussion thus far has been confined to the growth of perfect crystals. We have seen that thermal roughening can create large clusters that permit measurable growth on low-index planes. This effect can account for the rapid growth of dislocation-free silicon, for example (*4*). However, crystals can grow at low temperatures and small $\Delta\mu$ only when certain defects are present. I now discuss mechanisms involving dislocations and impurities.

A screw dislocation imposes a spiral-ramp structure on the layers of atoms in the crystal lattice (*2*). When the dislocation intersects a surface, one or more steps originate at the point of intersection (Fig. 6a). Steps correspond to the boundaries of incomplete layers and provide sites of high coordination that can serve as growth sites. Because of the topology of the defective lattice, the layers cannot be completed even as the crystal grows and steps are always present. The spiral mechanism is illustrated in Fig. 6. A dislocation with a double Burger's vector terminates at the center, and during growth the two associated steps wind up into a double spiral that expands to cover the face.

The simulated growth rates of a face intersected by such a dislocation are shown in Fig. 7; for comparison, the growth rates of a perfect crystal are also shown (*29*). At the lower temperature ($kT/\phi = 0.25$) the presence of the screw dislocation does increase the crystal growth rate considerably, especially at small $\Delta\mu$. Measurable growth is obtained at much smaller values of $\Delta\mu$. A simplified theoretical treatment of spiral growth (*30*) predicts that the growth rate R is proportional to $(\Delta\mu)^2$, but the data in Fig. 7 are described more accurately by the relation $R \propto (\Delta\mu)^{2.2}$. This difference is caused by the additional contribution of nucleation at the higher values of $\Delta\mu$ (*31*). Crystal growth rates are often characterized by the best exponent n in the relation $R \propto (\Delta\mu)^n$. Experimental studies seldom yield the integer values predicted by most theories. These results suggest that nonintegral values of n may result from data taken in a range of $\Delta\mu$ where several mechanisms are operative.

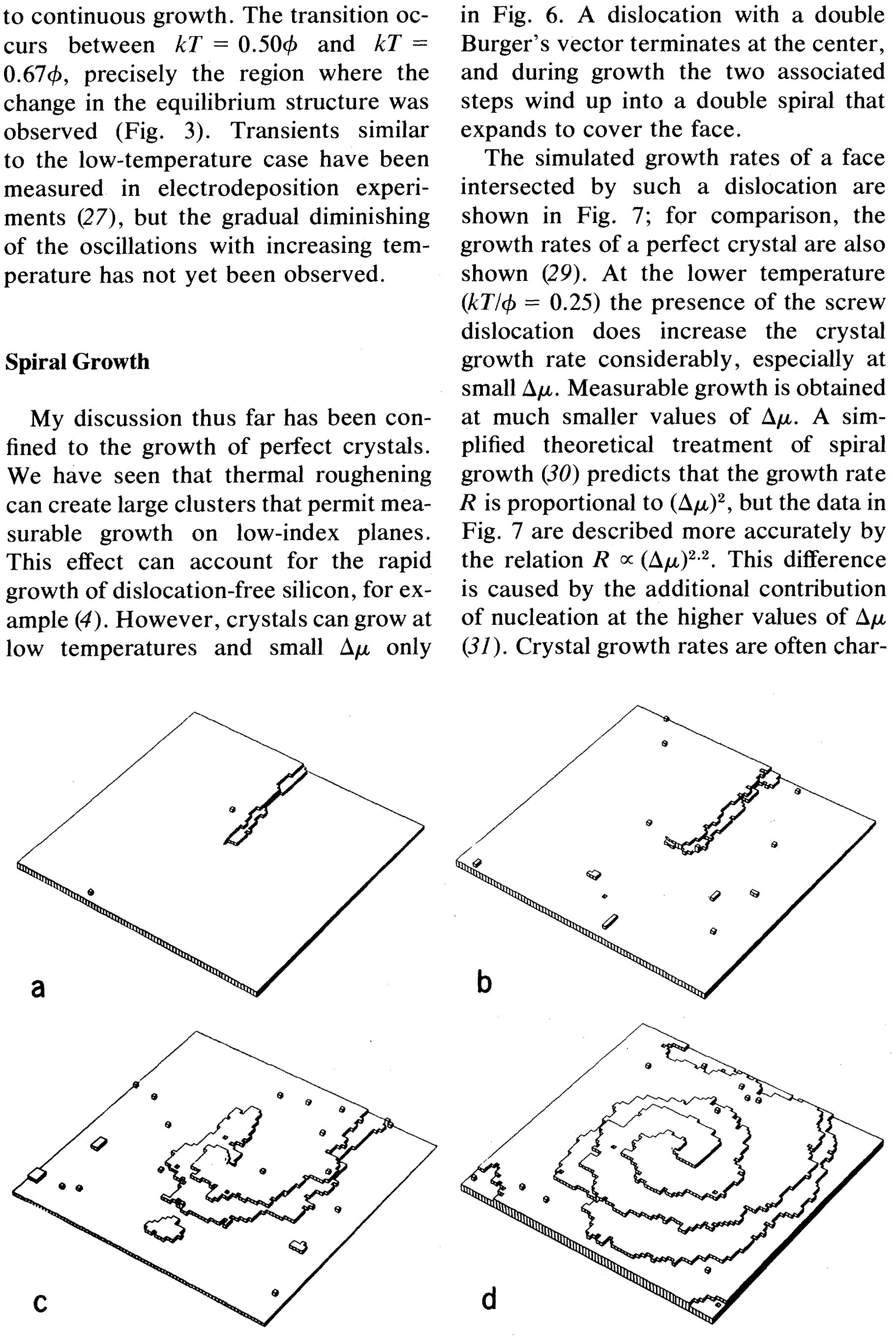

Fig. 6. The formation of a spiral step pattern is illustrated on an sc (100) face. A single screw dislocation intersects the surface segment at the center, and at this point two steps originate. In equilibrium the two steps are essentially straight, but, when the driving force is applied, they advance and eventually can provide a dense array of edge sites over a macroscopic crystal face.

Impurities

Deposition on close-packed faces may also be enhanced by the presence of impurities. For the present purpose, an impurity may be defined as any species except the primary component in the crystal. There are a number of practical uses for impurities; for example, hydrogen and chlorine are commonly used to facilitate the deposition of silicon at temperatures far below the melting point (*32*). Even minute quantities of specific materials can have drastic effects on the kinetics of crystal growth (*33*). Because of the difficulty of controlling the quantity of impurities and determining the location, the function of impurities is still not well understood. Simulation models, however, are ideally suited for impurity studies. All of the parameters that define the system are known, including the exact location of each impurity atom.

In general, impurities will enhance the interface mobility if they tend to increase the binding energy of a host atom to the surface. The decisive influence of this binding energy is evident in the comparative kinetics of the fcc (111) and (100) faces shown in Fig. 2a. Impurities may increase this energy in one of two ways. (i) An impurity that forms a strong bond to the host atom will adhere to the crystal surface and afford favorable sites for the adsorption of host atoms in its vicinity. (ii) A volatile impurity that forms a monolayer on the surface can stabilize host atoms simply through the provision of a large number of impurity-host bonds.

The kinetics of the sc (100) face with the first type of impurity are shown in Fig. 8 (triangular symbols) (*31*). In this case $\phi_{AB} = 2\phi_{AA}$, and $\phi_{AA} = \phi_{BB}$; ϕ_{AB}, ϕ_{AA}, and ϕ_{BB} are the energies of bonds between the atoms indicated by the subscripts. Here A corresponds to the host atom and B to the impurity. In this case the flux of B atoms from the vapor was $k_B{}^+ = 2.5 \times 10^{-3} k_A{}^+$, a rather small value. These impurities tend to be surrounded by A atoms in the crystal, because of the large AB bond energy, and form an ordered alloy when present in large quantities.

As might be expected, these impurities are most effective at small values of $\Delta\mu$.

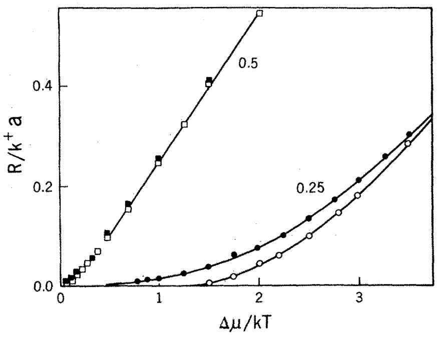

Fig. 7. The steady-state growth rates of surfaces intersected by a screw dislocation (closed symbols) are compared with the growth rates of perfect crystal surfaces (open symbols). The numbers adjacent to the curves indicate the value of kT/ϕ. The low-temperature data were obtained with a screw dislocation that has two associated steps, as shown in Fig. 6, whereas the high-temperature data were calculated with a dislocation that has four steps.

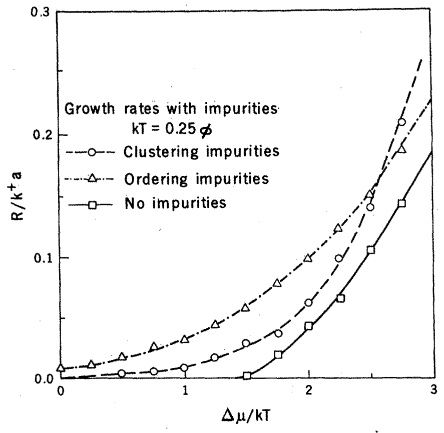

Fig. 8. Growth rates in the presence of impurities are compared with the growth rates of the pure crystal. (Dislocations are excluded in all cases.) The chemical potential of the ordering impurities was maintained at the value $\mu_B = \mu_A - 6\ kT$, whereas that for the clustering impurities was fixed at $\mu_B = \mu_B^{(e)} - 0.5\ kT$, where $\mu_B^{(e)}$ is the value required for equilibrium with a crystal composed of B atoms. Here $\Delta\mu = \Delta\mu_A = \mu_A - \mu_A^{(e)}$.

Here the slow nucleation rate suppresses the growth of the pure crystal, and even a very small flux of impurities will cause a large increase in the number of critical nuclei. At large values of $\Delta\mu$ where the nucleation rate exceeds k_B^+, there is little effect.

A finite growth rate is observed even when $\Delta\mu \rightarrow 0$. This is possible because the impurities occasionally impinge on vacant sites in the exposed close-packed layer of atoms. As the concentration of impurities increases in this layer, the stability of clusters on the surface is increased. Thus, the gradual transformation of the surface layers allows slow growth even under conditions where the pure crystal is in equilibrium. The value of $\Delta\mu$ plotted here is the difference between μ_A and the equilibrium value for a pure crystal, whereas the presence of the B atoms actually produces a more stable crystal with a lower vapor pressure. Thus, the value of $\Delta\mu$ required for equilibrium is somewhat negative when these impurities are present.

A very different mode of crystal growth can operate when clustering impurities are present; that is, when $\phi_{AB} < (\phi_{AA} + \phi_{BB})/2$. The weak AB bond tends to favor the aggregation of like atoms. Crystals composed of approximately equal quantities of A and B atoms usually exhibit phase separation below a critical mixing temperature T_M. Macroscopic regions are formed that are rich in either the A or the B component.

Clustering impurities may segregate at the crystal surface when the B component is more volatile; that is, when $\phi_{BB} < \phi_{AA}$. Optimum bonding is obtained with the A atoms occupying the interior sites where all of their bonds are saturated and with the B atoms at the surface. The relative sizes of the A and B atoms may also affect segregation in some systems, but the Ising model does not account for different atomic sizes (*34*).

A layer of impurity can adhere to the surface even when the concentration in the vapor is below the bulk precipitation value; that is, $\mu_B < \mu_B^{(e)}$. This is evident, at least at low temperatures, from the following kinetic argument. An impurity monolayer can be deposited, in principle, by the addition of atoms to kink sites. The monolayer kink site has m neighbors in the layer beneath, A atoms, and $(Z/2 - m)$ neighbors in the impurity layer. The kink site evaporation rate is $\nu \exp\ [m\phi_{AB}/kT - (Z/2 - m)\phi_{BB}/kT]$, which, for stability, must be equal to $k_B^+ = \nu e^{\mu_B/kT}$. Equating these rates, we obtain

$$\mu_B = \mu_B^{(e)} - m(\phi_{AB} - \phi_{BB}) \qquad (4)$$

where $\mu_B^{(e)} = -3\phi_{BB}$. Thus, when $\phi_{AB} > \phi_{BB}$, the chemical potential μ_B required to stabilize the impurity layer is less than the bulk precipitation value. Impurity layers of finite thickness will also be present for larger values of μ_B which are less than $\mu_B^{(e)}$.

This argument is valid at low temperatures, where the bulk of the crystal contains few B atoms and the monolayer contains few A atoms. More complete analyses (*35*) indicate that the surface composition changes abruptly from an A-rich layer to a B-rich layer as μ_B increases. The change is discontinuous when the temperature is smaller than a critical point that is approximately equal to the 2d AB critical mixing temperature, $T_M^{(2d)}$.

The kinetics of an sc (100) face with a layer of clustering impurities are also included in Fig. 8. Here, $\phi_{AB} = 0.533\ \phi_{AA}$, and $\phi_{BB} = 0.4\phi_{AB}$. Again, the impurities enhance the growth rate, especially at small values of $\Delta\mu$. Note the apparent linear dependence of R on $\Delta\mu$ for small values of $\Delta\mu$. This implies that nucleation is not required when clustering impurities cover the surface. Also, the impurity mechanisms clearly dominate the other modes of growth at small values of $\Delta\mu$. Thus, spiral kinetics are not the fastest mode of crystal growth for small $\Delta\mu$, since the parabolic dependence on $\Delta\mu$ leads to a very small growth rate in this region.

The kinetics of the segregated surface are similar to those associated with thermally roughened surfaces. The growth rates are much smaller, but this is to be expected since there are only a few sites where an A atom has a large binding energy to the crystal. Most sites in the surface layer are occupied by impurities, and the weak ϕ_{AB} bonds alone do not provide a large binding energy. Only those atoms that impinge on vacant sites in the surface layer have a high probability of being captured by the growing crystal.

Although the data of Fig. 8 are consistent with the idea that the layer of impurities causes roughening of the crystal surface, the transient data of Fig. 9 are not compatible with this notion. These data are the average growth rates subsequent to the application of the driving force $\Delta\mu = 2\ kT$. Initially the crystal was in equilibrium with a vapor that included impurities. The presence of oscillations implies that the interface was highly localized in the equilibrium state. In fact, the amplitude of the oscillations is actually larger than that observed for the pure crystal (Fig. 5) at any temperature. This suggests that the segregated surface remains localized for a longer time than the pure crystal surface.

The layer of volatile impurities acts in a manner analogous to a thin layer of liquid on the surface of the crystal. In equilibrium the concentration of A atoms in the layer is small, but, when $\Delta\mu$ is applied ($\mu_A > \mu_A^{(e)}$), the concentration gradually increases. The A atoms either replace the impurities or promote them to the next layer. Eventually the A atoms predominate in the layer. A new layer of impurities condenses, and the process repeats itself. The surface remains relatively flat because the clustering of A atoms is less pronounced with the impurities present.

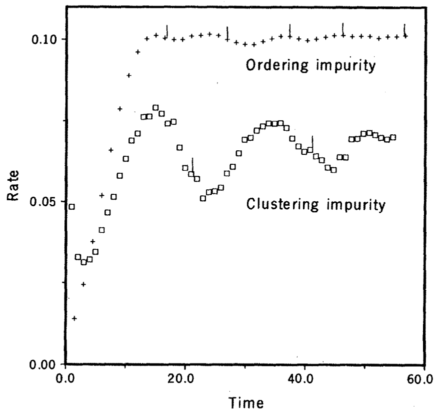

Fig. 9. Transient growth rates of crystals in the presence of ordering (crosses) and clustering (squares) impurities. In both cases $\Delta\mu_A = 2\ kT$, but $\mu_B = \mu_A - 6\ kT$ and $\mu_B = \mu_B^{(e)} - 0.5\ kT$ for the ordering and clustering impurities, respectively.

The operation of the surface segregation mechanism is rather sensitive to the detailed interactions between the host and impurity atoms. In the simulation described above, the segregated layer in equilibrium consists of approximately 20 percent A atoms, 75 percent B atoms, and 5 percent vacant sites. The growth rate is limited primarily by the rate at which A atoms impinge on the vacant sites, and for this reason a relatively volatile impurity is effective. Another factor to consider is the value of $T_M^{(2d)}$ for the segregated layer. Operation below this point will produce nucleation kinetics, since A-rich clusters would then have to be nucleated.

Also shown in Fig. 9 are the transient growth rates of the crystal with the ordering impurity. In this case, the initial vapor did not contain the impurity; at $t = 0$ the vapor pressure of the A component was increased to give $\Delta\mu_A = 2\ kT$ and the impurity was introduced into the vapor. The small initial rates indicate that few of the atoms stick at first. In fact, the initial rise in the growth rate is almost identical to that plotted in Fig. 5 ($kT/\phi = 0.25$), and this result is not surprising since the initial states of the two crystals are identical. However, subsequent oscillations are almost entirely absent when the ordering impurity is present. This indicates that the interface rapidly assumes a multilevel structure, and certainly the enhanced nucleation of clusters around the impurities should facilitate the spreading of the interface. Impurity atoms may impinge on the top of small clusters in the first layer and thus initiate clusters in the second layer before the first layer is even approaching completion. Again, it is apparent that ordering impurities promote growth through a qualitatively different mechanism from segregating impurities.

The composition of a crystal grown with impurities may differ substantially from the values corresponding to equilibrium phase diagrams. At large values of $\Delta\mu$, the more volatile component is trapped in excess of the equilibrium concentration (*36*). This occurs because this component impinges at the interface relatively fast as a result of its high vapor pressure, but the rapid motion of the interface permits insufficient time for evaporation of the atoms and many are trapped in the crystal. This effect may be enhanced when a layer of the volatile component segregates at the surface, and rapid growth may trap portions of this layer in the crystal.

Simulation data for the amounts of the impurity incorporated are shown in Fig. 10. A steep initial rise in the concentration of B atoms (clustering impurity) with $\Delta\mu$ is apparently the result of the relatively stable monolayer of B atoms at the surface. Also plotted are data for an ideal alloy impurity with $\phi_{AB} = (\phi_{AA} + \phi_{BB})/2$, but with the same value of ϕ_{AB} and approximately the same equilibrium concentration. The initial rise is much more gradual in this case, where segregation does not occur.

The concentration of clustering impurities captured by the crystal can exceed the maximum solubility of the B atoms in the A-rich region. The data of Fig. 10 indicate that $C_B = 0.13$ at $\Delta\mu/kT = 0.5$, whereas the maximum equilibrium concentration at this temperature is $C_B^{(e)} \cong 0.02$; when larger amounts of impurity are present, the system will eventually precipitate the B-rich phase. Thus, the kinetics of the growth process have produced a metastable alloy. Since the B-rich phase can only be created by a nucleation event, the metastable system may remain indefinitely in the supersaturated condition. A small solid-state diffusion coefficient also slows the precipitation process. New techniques of crystal growth that generate very large values of $\Delta\mu$ have produced metastable systems with impurity concentrations that exceed the equilibrium value by several orders of magnitude (*37*). With techniques of this sort available, a whole new class of materials can be constructed with new and perhaps useful properties.

The enhanced rate of impurity capture in the presence of a segregated layer may explain variations in impurity capture on different close-packed faces of a single crystal. Certain minerals and artificially grown crystals exhibit sectors of high impurity concentration that correspond to the regions of the crystal deposited on specific low-index faces (*38*). Since the surface layers along different low-index orientations have different binding energies for impurities, it is apparent that the driving force for segregation may depend on orientation. Thus, some orientations may contain B-rich monolayers, whereas others do not. The results in Fig. 10 suggest that the capture of impurities will be significantly greater on surfaces containing the B-rich layer.

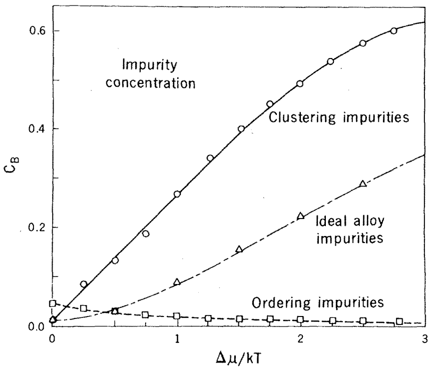

Fig. 10. The concentration of impurity trapped in the crystal. The square and circular symbols correspond to the ordering and clustering impurities, respectively, under precisely the conditions specified in Fig. 8.

The ordering impurities are incorporated in the greatest numbers at small values of $\Delta\mu$. These impurities are more likely to stick than the host atoms, especially at small values of $\Delta\mu$ where the probability of an atom sticking is very small. As $\Delta\mu$ is increased, few impurity atoms impinge on a given layer of the crystal and the concentration is reduced. In general, an increase in $\Delta\mu$ causes an increase in the impurity concentration when $\phi_{AB} < \phi_{AA}$ and a decrease when $\phi_{AB} > \phi_{AA}$.

Final Remarks

Computer simulations of the kinetic Ising model have demonstrated that a number of factors influence the motion of the interface. Important are the arrangement of the atoms at the surface, the surface temperature, screw dislocations, and impurities. In addition, although not discussed above, simulations have shown that the growth rates are sensitive to the mobility of atoms parallel to the interface (*39*). At the present time, simulations are the most effective method of treating dynamic systems of this kind, where complex phase transitions play an important role.

Practical benefits must result from a

better understanding of the kinetics of the interface. For example, thin, polycrystalline metallic films are applied to numerous devices to prevent corrosion and to provide conducting paths. A smooth film of uniform thickness is desirable for most purposes. But, since the kinetics of deposition are usually anisotropic, different crystallites in the film will thicken at different rates and produce a coarse and irregular structure. From the discussion above, we see that the conditions can be modified in several ways to reduce the kinetic anisotropy. (i) The temperature can be increased to exceed the roughening point of all faces. (ii) The driving force can be increased (Fig. 2a). (iii) Impurities can be added to the system to facilitate nucleation on close-packed faces. In practice, impurities are often used for this purpose, but a better understanding of the exact role of the impurity may facilitate the search for the most effective agent.

The Ising model is well suited to a study of interface kinetics. It is probably the simplest model that can exhibit the basic phenomena of surface roughening, impurity segregation, and lattice defects. It is equivalent to the Kossel model discussed by Volmer (*10*) and Stranski (*11*) many years ago. However, only recently has the computer technology been developed that has enabled us to evaluate its properties in some detail. Improvements in the model are needed, in order to treat other important aspects of crystal growth. Models that allow continuous atomic coordinates can exhibit the formation of lattice defects during the crystal growth process. Also, an accurate treatment of the crystal-melt interface kinetics requires a more detailed model. Thus, although considerable progress has been achieved, a number of interesting problems remain to be solved.

References and Notes

1. R. Becker and W. Döring, *Ann. Phys. (Leipzig)* **24**, 719 (1935).
2. F. C. Frank, *Discuss. Faraday Soc.* **5**, 48 (1949); *ibid.*, p. 67.
3. H. Bethge, K. W. Keller, E. Ziegler, *J. Cryst. Growth* **3/4**, 184 (1968); C. Kimura, T. Yanaki, H. Hoshino, *ibid.*, **38**, 233 (1972); K. Sato and M. Okada, *ibid.* **42**, 264 (1977).
4. Dislocation-free silicon, for example, grows from the melt with only a small undercooling below the melting point [see T. F. Ciszek, *J. Cryst. Growth* **10**, 263 (1971)].
5. Color movies of crystal growth simulations have been produced. *Computer Simulation of Crystal Growth* by G. H. Gilmer, K. C. Knowlton, H. J. Leamy, and K. A. Jackson contains Ising model simulations of nucleation, continuous spiral growth, and two impurity mechanisms. Particles interacting by Lennard-Jones potentials are deposited onto a substrate in *Nucleation on a Crystal Surface* by G. H. Gilmer, K. C. Knowlton, M. Shugard, and J. C. Tully. Both movies are available for loan; inquiries should be directed to Film Library, Bell Laboratories, Murray Hill, N.J. 07974.
6. The Ising model and its application to crystal-vapor systems are treated in K. Huang, *Statistical Mechanics* (Wiley, New York, 1963).
7. J. M. Hammersley and D. C. Handscomb, *Monte Carlo Methods* (Methuen, London, 1964).
8. T. L. Hill, *An Introduction to Statistical Thermodynamics* (Addison-Wesley, Reading, Mass., 1960).
9. H. J. Leamy, G. H. Gilmer, K. A. Jackson, in *Surface Physics of Materials*, J. B. Blakeley, Ed. (Academic Press, New York, 1975), vol. 1, p. 121.
10. M. Volmer, *Die Kinetik der Phasenbildung* (Steinkopf, Dresden, 1939).
11. I. N. Stranski, *Z. Phys. Chem.* **136**, 259 (1928).
12. G. H. Gilmer and K. A. Jackson, in *Crystal Growth and Materials*, E. Kaldis and H. J. Scheel, Eds. (North-Holland, Amsterdam, 1977), p. 80. Additional fcc rates are in U. Bertocci, *J. Cryst. Growth* **26**, 219 (1974).
13. R. Uyeda, *J. Cryst. Growth* **24/25**, 69 (1974). Similar shapes result from vapor deposition on substrates [see K. Heinemann, M. J. Yacaman, C. Y. Yang, H. Poppa, *ibid.* **47**, 177 (1979)].
14. A detailed comparison of nucleation rates and theory on the sc (100) face is given by J. D. Weeks and G. H. Gilmer [*Adv. Chem. Phys.* **40**, 157 (1979)].
15. A. I. Michaels, G. M. Pound, F. F. Abraham, *J. Appl. Phys.* **45**, 9 (1974).
16. W. K. Burton and N. Cabrera, *Discuss. Faraday Soc.* **5**, 33 (1949).
17. K. A. Jackson, in *Liquid Metals and Solidification* (American Society for Metals, Metals Park, Ohio, 1958), p. 174.
18. J. W. Cahn and J. E. Hilliard, *J. Chem. Phys.* **28**, 258 (1958); J. W. Cahn, *ibid.* **30**, 1121 (1959).
19. D. E. Temkin, *Sov. Phys. Crystallogr.* **14**, 344 (1969).
20. F. F. Abraham and G. H. White, *J. Appl. Phys.* **41**, 1841 (1970); V. V. Solovev and V. T. Borisov, *Sov. Phys. Dokl.* **17**, 8 (1972).
21. G. H. Gilmer and P. Bennema, *J. Appl. Phys.* **43**, 1347 (1972); S. W. H. de Haan, V. J. A. Meeussen, B. P. Veltman, P. Bennema, C. van Leeuwen, G. H. Gilmer, *J. Cryst. Growth* **24/25**, 491 (1974).
22. J. D. Weeks, G. H. Gilmer, H. J. Leamy, *Phys. Rev. Lett.* **31**, 549 (1973).
23. S. T. Chui and J. D. Weeks, *Phys. Rev. B* **14**, 4978 (1976).
24. H. van Beijeren, *Phys. Rev. Lett.* **38**, 993 (1977); H. J. F. Knops, *ibid.* **39**, 766 (1977).
25. K. A. Jackson and C. E. Miller, *J. Cryst. Growth* **40**, 169 (1977).
26. A. Pavlovska, *ibid.* **46**, 551 (1979).
27. A. Bewick, M. Fleischmann, H. R. Thirsk, *Trans. Faraday Soc.* **58**, 2200 (1962). Crystals apparently free of screw dislocations were examined by V. Bostanov, R. Roussinova, and E. Budevski [*J. Electrochem. Soc.* **119**, 1346 (1972)].
28. G. H. Gilmer, *J. Cryst. Growth*, in press.
29. ———, *ibid.* **35**, 15 (1976); R. H. Swendsen, P. J. Kortman, D. P. Landau, H. Müller-Krumbhaar, *ibid.*, p. 73.
30. N. Cabrera and M. M. Levine, *Philos. Mag.* **1**, 450 (1956).
31. G. H. Gilmer, *J. Cryst. Growth* **42**, 3 (1977).
32. A. A. Chernov, *ibid.*, p. 55.
33. R. J. Davey and J. W. Mullin, *ibid.* **26**, 45 (1974).
34. F. F. Abraham, N.-H. Tsai, G. M. Pound, *Surf. Sci.* **83**, 406 (1979).
35. C. R. Helms, *ibid.* **69**, 689 (1977).
36. A. A. Chernov, *Sov. Phys. Usp.* **13**, 101 (1970).
37. H. J. Leamy, J. C. Bean, J. M. Poate, G. K. Celler, *J. Cryst. Growth* **48**, 379 (1980).
38. L. S. Hollister, *Am. Mineral.* **55**, 742 (1970).
39. See (*21*) and (*29*) for simulations that include surface diffusion. For a general review of the theory of crystal growth, see (*14*); H. Müller-Krumbhaar, in *Current Topics in Materials Science* (North-Holland, Amsterdam, 1978), vol. 1, p. 1; vol. 2, p. 115. For a survey of Monte Carlo simulations, see (*12*); J. P. van der Eerden, P. Bennema, T. A. Cherepanova, in *Progress in Crystal Growth and Characterization*, B. R. Pamplin, Ed. (Pergamon, Oxford, 1979), vol. 3, p. 219.
40. I thank J. D. Weeks, K. A. Jackson, and H. J. Leamy for collaboration on most of the work reviewed here.